Journal of Sol-Gel Science and Technology (2018) 85:677–683
https://doi.org/10.1007/s10971-018-4598-x

ORIGINAL PAPER: SOL-GEL AND HYBRID MATERIALS FOR CATALYTIC, PHOTOELECTROCHEMICAL AND SENSOR APPLICATIONS

Preparation and characterization of the system $NiMn_2O_4/TiO_2$ by sol–gel: application to the photodegradation of benzamide under visible light

Gharib Rekhila[1] · Yamina Gabes[1] · Razika Brahimi[1] · Yassine Bessekhouad[1,2] · Ousama Mahroua[1] · Mohamed Trari[1]

Received: 6 November 2017 / Accepted: 24 January 2018 / Published online: 15 February 2018

Abstract

Benzamide is successfully degraded on the novel heterosystem $NiMn_2O_4/TiO_2$ under visible light. The nanosized spinel is synthesized by the sol–gel method at ~850 °C. The X-ray diffraction pattern shows narrow peaks and the oxides are well crystallized. The Mott–Schottky plot ($C^{-2}-E$) of $NiMn_2O_4$ is characteristic of *p*-type conductivity from which a flat-band potential of −0.20 V_{SCE} is obtained. The energy-band diagram, built from the physicochemical characterizations, predicts the electron transfer from the conduction to dissolved oxygen via TiO_2. The loading of TiO_2 with $NiMn_2O_4$ enhances the photoactivity and $NiMn_2O_4$ islands achieve a colloidal photochemical heterosystem, tested successfully for the light-induced benzamide degradation. The spinel dose and benzamide concentration are optimized. Under the ideal conditions, the rate of the benzamide disappearance is controlled by high-performance liquid chromatography. A conversion of 85% is reported in aerated benzamide solution (15 ppm) in less than 2 h under artificial light. This conversion rate increases up to 94% under solar light and the oxidation obeys to a first-order kinetics with a half-life of 53 min.

Graphical Abstract

Photodegradation of benzamide on the heterosystem $NiMn_2O_4/TiO_2$ under visible light.

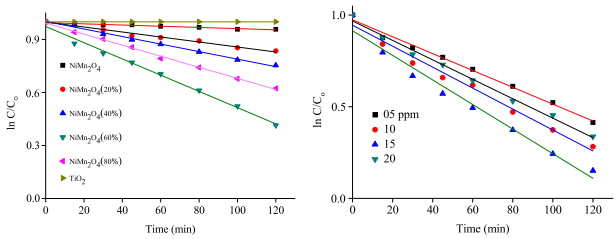

Keywords Benzamide · Nanosized spinel · Sol–gel · Heterosystem $NiMn_2O_4/TiO_2$ · Photocatalytic degradation · Sunlight

Highlights

- The benzamide was photodegraded on the hetero-system $NiMn_2O_4/TiO_2$ synthesized by sol gel.
- The direct optical transition (1.75 eV) makes the spinel $NiMn_2O_4$ attractive for the light energy conversion.
- The benzamide elimination, controlled by HPLC, follows a first order kinetic with a rate half-life of 53 min.
- The improved photocatalytic performance is due to the electrons transfer $NiMn_2O_4/TiO_2$.

✉ Gharib Rekhila
rekhilagharib@gmail.com

[1] Laboratory of Storage and Valorization of Renewable Energies, Faculty of Chemistry (USTHB), BP 32, 16111 Algiers, Algeria

[2] National Veterinary High School, BP 161, Algiers, Algeria

1 Introduction

The aquatic environment polluted by dyes and pesticides is conventionally treated by physical and/or biological techniques which reduce the pollution level, but are not enough to reach the threshold required by the water standards [1–4]. The advanced oxidation process (AOP) is an attractive technique for water depollution, particularly for the effluents of the pharmaceutical industry [5–7]. In this respect, the semiconductor–liquid junction, assimilated at microphotoelectrochemical (PEC) cells, can be used as a photocatalytic system able to decontaminate polluted water [8–10]. The spinels based on *3d* metals are photocatalysts of choice which begin to gain popularity in the solar energy conversion owing to their chemical stability, nontoxicity, and absorption in the solar spectrum [11, 12]. Under irradiation, they can degrade organic pollutants because the potential of their conduction band is above the $O_2/O_2^{\bullet}$ couple [13, 14], produce hydrogen [15], or reduce heavy metals to element states [16].

With a forbidden band of ~2 eV, the spinels MM'_2O_4 absorb ~40% of the solar light; M and M′ belong to the first row of transition metals. The optical transition is of *d–d* characteristic, it involves lower and upper bands of *3d* orbitals coming from the crystal field splitting, and consequently, the photocorrosion is inhibited in aqueous electrolytes [17, 18]. In addition, the band position does not change with pH and can be adequately positioned with respect to redox levels in solution by a judicious choice of pH.

This work is a systematic investigation of the photocatalysis for the degradation of organic molecules (drugs, pesticides, and dyes) in our laboratory [19]. The aim of the present contribution is to report the synthesis and characterization of the spinel $NiMn_2O_4$ by sol–gel method and the PEC properties. The technique involves the precursor hydrolysis and a polycondensation to glass-like form. The reagents are mixed at an atomic scale and this should accelerate the reaction rate, leading to the nanocrystallite formation. As an application, the photocatalytic performance is tested through the oxidation of benzamide, a recalcitrant molecule on the heterosystem $NiMn_2O_4/TiO_2$ upon visible light. The activity is dependent on some parameters such as the sensitizer dose, the benzamide concentration, and pH. The benzamide oxidation was monitored by high-performance liquid chromatography (HPLC) and the conversion rate reached 94% under solar light.

2 Experimental

$NiMn_2O_4$ was prepared by sol–gel method; the detailed procedure was reported elsewhere [20]. Briefly, stoichiometric amounts of $Ni(NO_3)_3{\bullet}7H_2O$ (Merck, 99.5%) and Mn $(NO_3)_2{\bullet}6H_2O$ (Merck, 99.5%) were dissolved in water containing the gelling agent (Agar-Agar Flucka, 1 g L^{-1}). The solution was heated at 70 °C and the gel was dehydrated at 130 °C under magnetic stirring on a hot plate until apparition of a gray color. At this level, the particles are dispersed in the solvent, and a colloidal suspension is formed. Then, the colloids in the solvent are linked by sol condensation, to form a three-dimensional open grid (gel) and this constitutes the gelation process. Finally, the sample was ground in an agate mortar and heated at 850 °C (18 h) in a muffle furnace with intermediate regrinding, the end product exhibits a black color.

The thermogravimetry analysis (TG) was performed in air at a heating rate of 3 °C min^{-1} using a thermobalance (Setaram, Setsys 16/18). TiO_2 was prepared according to our previous work [21, 22]. The formation of the phases was confirmed by X-ray diffraction (XRD) over the 2θ range (15–100°) using a Siemens diffractometer (Model D-5000). The FTIR analysis was conducted on a pressed pellet using 1 mg of the spinel dispersed in 150 mg of KBr of spectroscopic quality. The TEM image was taken with a Hitachi S2500. The diffuse reflectance was determined with a UV-Visible spectrophotometer (Specord 200 Plus). The photoactivity was tested through the degradation of benzamide. The experiments were performed in a Pyrex reactor equipped with a cooling system whose temperature was maintained at 25 °C. The tests were done in batch mode at neutral pH using 100 mL of benzamide solution at different concentrations (5–20 mg L^{-1}) and variable spinel doses $\{Y\% = x/(x + 125) \times 100\}$, x is the mass of NiM_2O_4, while the mass of TiO_2 (Riedel-de-Haën) is maintained constant (125 mg).

Before irradiation, the mixture was sonicated for 2 min in order to disperse the catalysts and maintained in the dark for 1 h to reach the absorption equilibrium. The catalyst powder was dispersed by magnetic agitation (200 rpm) using a double-walled Pyrex reactor with 0.5 cm of water which absorbs the IR radiation. The artificial light (Tungsten lamp: 5 mW cm^{-2}), measured with a calibrated light meter (Testo 545) and solar irradiation, was used as light sources.

Aliquots (0.5 mL) of the solution were withdrawn at regular time intervals and subjected to filtration to separate the solid particles and analyzed. The remaining concentration of benzamide was titrated by HPLC equipped with a C18 column. An aliquot of 10 µL of solution were filtered through a 0.45-mm Millipore filter (Whatmann) and injected in the chromatograph (Jasco PC1201). The wavelength of the maximum absorption (618 nm) was taken from the UV-Vis spectrum. The photocatalytic yield was calculated from the relation

$$\eta = 100 \times (C_o - C_t)/C_o, \quad (1)$$

where C_o is the initial concentration and C_t the concentration after irradiation for time (t); no benzamide was

degraded by photocatalysis. The solutions were made up with CO_2-free distilled water (conductivity ~0.7 MΩ cm).

3 Results and discussion

TG analysis was undertaken to delimit the temperature domain of the synthesis and thermal stability of the spinel; Fig. 1 shows the TG plot of the nitrate mixture in air obtained just after water vaporization. The mass decreases slightly up to ~400 °C due to water removal after which it undergoes a drastic weight loss until ~520 °C followed by a second weight loss at ~690 °C attributed to nitrates decomposition. The weight levels of beyond 800 °C indicate the formation of the spinel. The DTG peak curve at ~770 °C confirms the synthesis temperature of $NiMn_2O_4$.

The prepared spinel is the single phase and crystallizes in a cubic symmetry (SG: Fd3m). All XRD peaks (Fig. 2) belong to the inverse spinel $Mn[NiMn]O_4$ and agree with the JCPDS cards N° 11-1110. The structure consists of a close-packed arrangement of O^{2-} ions with one-half of octahedral cavities occupied by Ni^{2+} and one-eighth of tetrahedral sites occupied by Mn^{3+} (Fig. 3a). The TEM image (Fig. 3b) gives an average grain size of 310 nm, which is greater than that calculated from the full width at half maximum (L ~63 nm, $=0.9\,\lambda\ (\beta\ \cos\theta)^{-1}$) and this clearly indicates the presence of agglomerates which form grains. The L-value gives an active surface area of ~18 $m^2\,g^{-1}$ $\{S_{sp} = 6\ (d_{exp}\ L)^{-1}\}$, assuming that compact crystallites with a spherical shape, d_{exp} (=5.01 g cm^{-3}) are the experimental density.

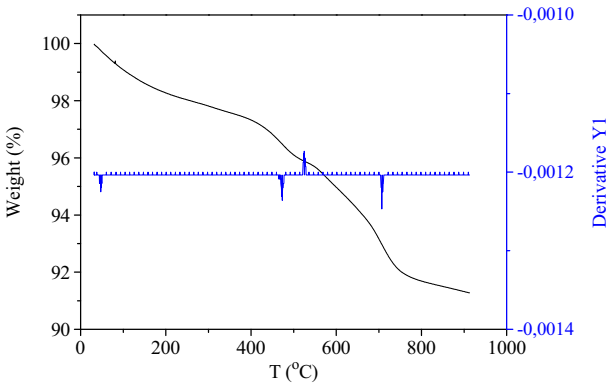

Fig. 1 TGA plot of the precursors indicating the formation of $NiMn_2O_4$ in air

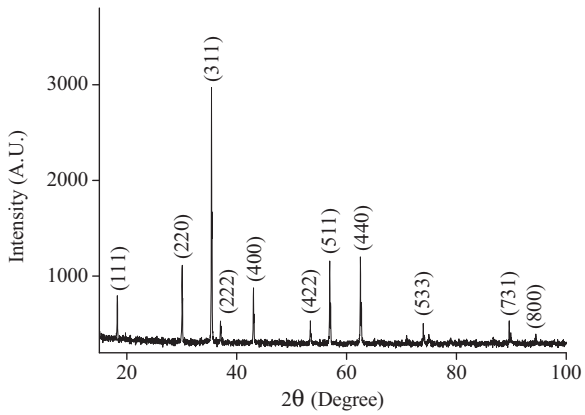

Fig. 2 The powder X-ray pattern of $NiMn_2O_4$

The optical properties of $NiMn_2O_4$ are typical of semiconductors and are therefore not different from those of other spinels [23, 24]. The absorption coefficients (α) and the incident energy ($h\nu$) are given by the Tauc relation

$$(\alpha h\nu)^n = \text{Cont} \times \left(h\nu - E_g\right), \tag{2}$$

where the exponent n depends on the type of transition: $n =$ 2 or 1/2, respectively, for indirect or direct transitions. The extrapolation of the straight line $(\alpha h\nu)^2$ to the energy axis shows a direct transition with an E_g value of 1.75 eV (Fig. 4).

The key parameter of a photocatalyst is its semiconductivity and the transport properties are undertaken for this purpose. The small electrical conductivity ($\sigma_{300\,K}$ ~10^{-5} $\Omega^{-1}\,m^{-1}$) is characteristic of semiconducting behavior with a low doping density (N_A) and an extended depletion width (δ), where the electron/hole (e^-/h^+) pairs are separated by the junction electric field (see below). The thermal variation $\sigma(T)$ follows an Arrhenius-type law with activation energy of 0.33 eV. This trend is confirmed by the positive thermopower ($+130\,\mu V\,K^{-1}$ at 300 K) which indicates that the majority of carriers are holes with a concentration of ~10^{18} cm^{-3}.

Benzamide is weakly dissociated and the intensity-potential $J(E)$ characteristic of $NiMn_2O_4$ electrode is plotted in neutral solution (pH ~7) using Na_2SO_4 (10^{-2} M) as a supporting electrolyte. The curve exhibits a plateau region with a dark current less than 0.2 mA cm^{-2} and which becomes cathodically large below −0.2 V, and the absence of a diffusion plateau indicates a water reduction. The spinel is known to produce hydrogen under illumination [25, 26]. The photocurrent (J_{ph}) appears at ~0.3 V (photocurrent onset potential V_{on}) and increases toward cathodic potentials, confirming the p-type behavior. However, the flat-band potential (E_{fb}) under the operating conditions is accurately obtained from the Mott–Schottky relation

$$\frac{1}{C^2} = \left(\frac{2}{\varepsilon\varepsilon_0 e N_A}\right)(E_{fb} - E - kT/e), \tag{3}$$

where ε (=50) is the dielectric constant of the spinel, ε_o is the dielectric constant of vacuum (8.85×10^{-12} F m^{-1}), e is the electron charge, N_A is the hole density, kT is the thermal energy (~26 meV at 300 K), and E is the applied potential. The intercept of the fitted line at $C^{-2} = 0$ (Fig. 5) and the

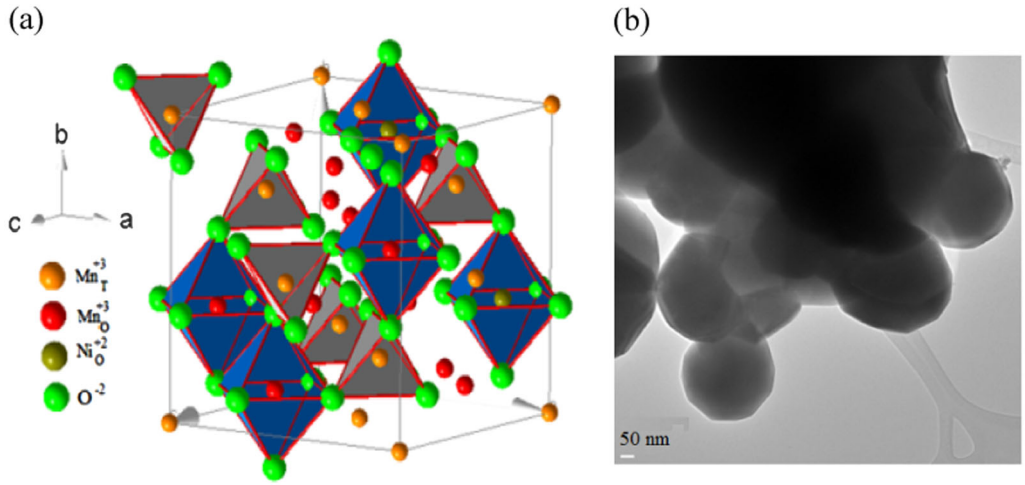

Fig. 3 **a** The spinel structure of $NiMn_2O_4$, T tetrahedral coordination, O octahedral coordination. **b** The TEM micrograph of $NiMn_2O_4$ prepared by sol–gel

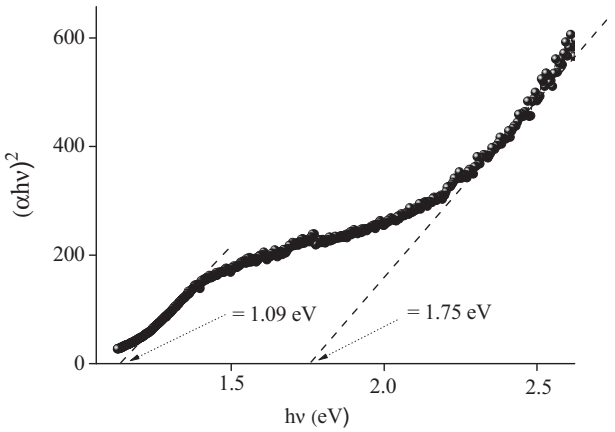

Fig. 4 Variation of $(\alpha h\nu)^2$ plot vs. the photon energy ($h\nu$) for $NiMn_2O_4$

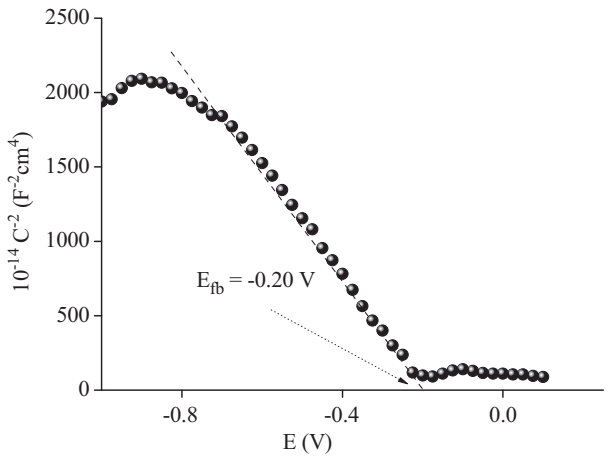

Fig. 5 The Mott–Schottky plot of *p*-type $NiMn_2O_4$

slope gives, respectively, the potential E_{fb} (−0.20 V) and holes density ($N_A = 1.3 \times 10^{16}\,cm^{-3}$); the N_A value produces an extended depletion width (δ ~400 nm) which is greater than the penetration depth (α^{-1}). The plateau region above −0.2 V corresponds to the accumulation zone with an increased recombination rate of (e^-/h^+) pairs, while the bending below −0.7 V is due to the inversion of electronic bands. The potentials of the valence (VB) and conduction band (CB) are crucial in photocatalysis and are given by

$$E_{CB} = 4.75 + e\,E_{fb} + 0.056\left(pH - pH_{pzc}\right) + E_a \quad (4)$$

$$E_{VB} = E_{CB} + E_g. \quad (5)$$

The activation E_a (~0.33 V) was determined from the conductivity measurements on sintered pellets. The value of CB (−3.13 eV/−1.62 V) and VB (−4.88 eV/0.13 V) indicates that both bands are made up of *3d* orbital ($t_{2g}-e_g$), which takes its origin from the crystal field splitting of *3d* metal.

3.1 Photocatalysis

The adsorption is widely used for the removal of organic molecules; however, it remains a displacement of the pollution and the used pollutant must be converted to less-harmful forms (ideally into CO_2 and H_2O) to regenerate the catalyst powder and this needs a further energy. By contrast, the environmental photoelectrochemistry is an emerging strategy for water decontamination [27, 28] and AOP requires radicals $O_2^{\bullet}$ and/or $OH^{\bullet}$ formed in the conduction and valence bands, respectively, which should destroy the organic matter. Accordingly, the presence of dissolved oxygen is necessary for the photocatalytic process. Indeed, it has been reported that the bubbling solution by nitrogen considerably inhibits the photoactivity [29].

Coupling two SCs with different energy levels, for the synergy, has been actively used. We have established the

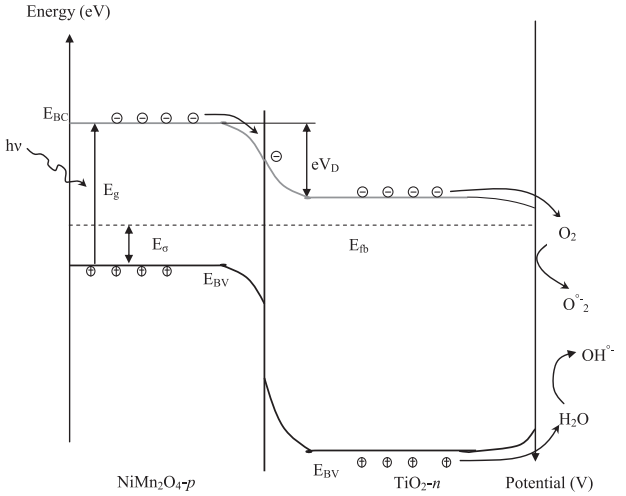

Fig. 6 The energy-band diagram of the heterosystem $NiMn_2O_4/TiO_2$

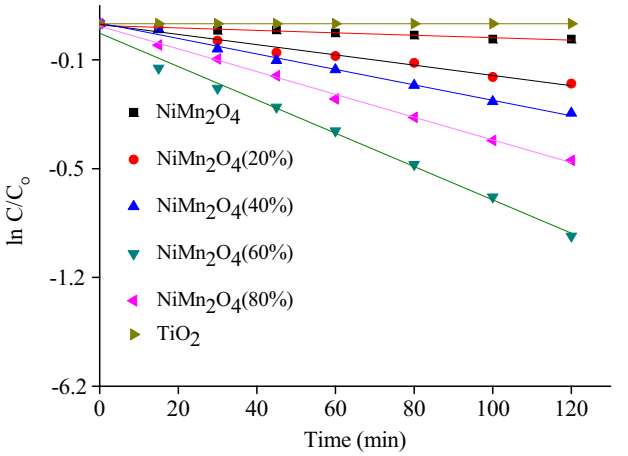

Fig. 7 The first-order kinetics model of $NiMn_2O_4/TiO_2$ heterosystem for benzamide degradation at different doses

energy diagram of the heterosystem $NiMn_2O_4/TiO_2$/benzamide solution on the basis of the physicochemical characterizations (Fig. 6). Generally, the radicals are formed on wide-band-gap semiconductors illuminated by UV light [30, 31]. The injection of charge carriers occurs isoenergetically and the large difference between $NiMn_2O_4$–CB of $O_2/O_2^{\bullet}$ level makes the electronic transfer weak, leading to a slow photocatalytic kinetics. So, TiO_2 is used as electrons bridge in order to mediate the electron transfer in solution.

As mentioned above, $NiMn_2O_4$–CB is made up of e_g orbital and is pH insensitive, whereas the electronic bands of TiO_2 change by $-0.06\,V\,pH^{-1}$, this property has been exploited to have an optimal band bending at the solid interface $NiMn_2O_4/TiO_2$ and this occurs around pH ~7. On the other hand, the photoactivity is dependent on the morphology of the catalyst and the effect of decreasing the crystallite size on benzamide oxidation is studied. The lifetime of the charge carriers must be long enough to reach the interface; nanosized dimension is desirable in such a case and the sol–gel is appropriate for preparing powders with increased surface-to-volume ratio. Moreover, the porosity of $NiMn_2O_4$ reduces the overpotential of the electrochemical reactions and increases the number of the photocatalytic sites.

The dark adsorption is a preamble for the photocatalysis of both organic and inorganic compounds. The isoelectric point (IP) of TiO_2 on which the adsorption occurs is obtained by the simple technique of powder addition [32], IP is found to be ~6.5, and the surface is positively charged at neutral pH. The resonance structure of benzamide occurs between the double bond and the lone pair of nitrogen and is likely responsible for binding which favors its access to catalytic sites of TiO_2 by electrostatic attraction.

Benzamide is not converted by photolysis, and ~5% is adsorbed as shown by measurement of the concentration before and after keeping the powder overnight in benzamide solution. Therefore, the decrease of the concentration is mainly attributed to the photocatalytic process; the reaction mechanism currently adopted under irradiation is the following [33]:

$$O_{2\,ads} + e^- \rightarrow O_2^{\bullet} + H^+ \rightarrow HO_2^{\bullet} \rightarrow H_2O_2(+e^-) \rightarrow O_2 + OH^{\bullet} + OH^- \quad (6)$$

$$O_2^{\bullet} + e^- \rightarrow O_2^{\bullet -}. \quad (7)$$

The illumination time is fixed at 2 h and the principal parameters influencing the photoactivity are the catalyst dose, pH, and benzamide concentration. As expected, the performance increases with increasing the amount of the sensitizer $NiMn_2O_4$ (Fig. 7) due to the large reception surface; this occurs because of the high number of PEC sites for the visible photons and in this way the generated (e^-/h^+) pairs. The first parameter was the spinel dose Y% ($=x/(x+125)\times 100$) which varies in the range (0–100%) while maintaining the amount of TiO_2 constant (125 mg). The optimal dose ($Y\%NiMn_2O_4/TiO_2$) under artificial light is found to be 60% for benzamide degradation (5 ppm) with a half-life of ~100 min. The regression in the activity above the threshold dose is due to the light obstruction of the catalyst powder and the shadowing effect. The normalized benzamide concentration vs. irradiation time is shown in Fig. 8; the linear dependence of the photocatalytic degradation indicates a first-order kinetics:

$$\mathrm{Ln}\,C_t = -kt + \ln C_o. \quad (8)$$

The half-life ($t_{1/2}$), the time needed to oxidize half of benzamide present initially, is found to be 2 h. In addition, the kinetics shows an initial period of relatively rapid

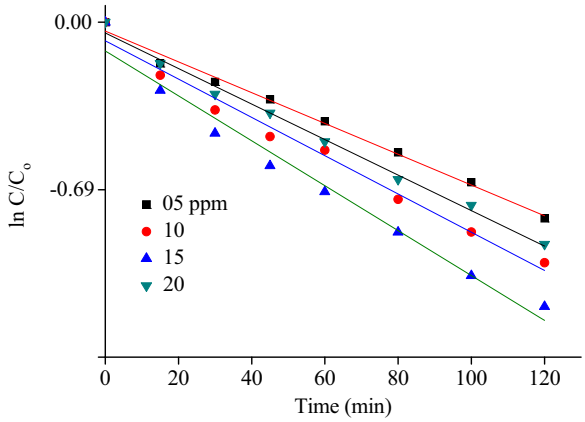

Fig. 8 The effect of the initial benzamide concentration toward the photoefficiency of $NiMn_2O_4/TiO_2$ heterosystem

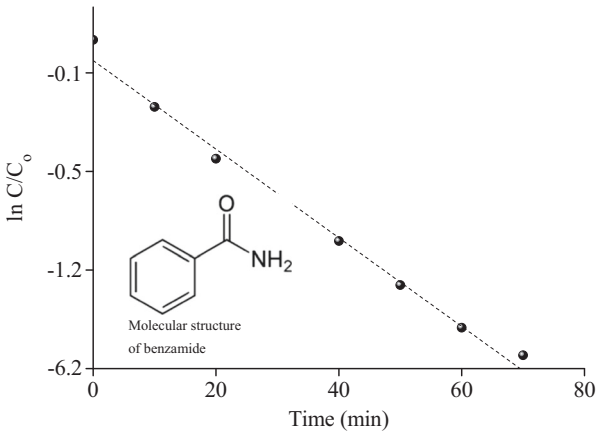

Fig. 9 Effect of solar light toward the efficiency of $NiMn_2O_4/TiO_2$ heterosystem. Experimental conditions: catalyst, $NiMn_2O_4$ (60%)/TiO_2; $[benzamide]_O = 15\ mg\ L^{-1}$; $V_{solution} = 50\ mL$; pH ~7

degradation. Over irradiation time, the slope decreases progressively, followed by gradual cessation. This tendency to saturation indicates that the layers already adsorbed are first oxidized after which the kinetics becomes governed by the diffusion of benzamide toward the active sites at the interface in which the radicals $O_2^{\bullet}$ are generated for further adsorption/photodegradation. This process is self-limited due to the adsorbed layer and the availability of photocatalytic sites. Such result implies an efficient contact by collision which facilitates the electron transfer between $NiMn_2O_4$ and TiO_2.

The photocatalytic performance under solar irradiation is strongly enhanced compared to artificial light (Fig. 9). Indeed, in addition to $NiFe_2O_4$, TiO_2 is activated under solar light which accounts for ~5% of UV light and the electron concentration is increased, leading to improved photoactivity up to 94%.

4 Conclusion

Benzamide is oxidized on the $NiMn_2O_4/TiO_2$ heterosystem under visible illumination. The nanosized catalyst is elaborated by sol–gel. The XRD exhibits narrow peaks and the oxide is well crystallized. The capacitance measurement ($C^{-2}-E$) of $NiMn_2O_4$ indicates *p*-type conductivity. The band gap and the flat-band potential permit to build the energy-band diagram which shows the electron transfer from the conduction to dissolved oxygen via TiO_2 and the degradation is considerably increased. The rate of benzamide degradation is monitored by HPLC and the spinel dose and benzamide concentration are optimized. The photoactivity is enhanced under solar light because of the activation of TiO_2. A conversion of 94% is reported in aerated benzamide solution (15 ppm) in ~1 h under sunlight and the oxidation follows a first-order kinetics with a half-life of 53 min.

Acknowledgements The authors would like to express their gratitude to the Faculty of Chemistry for financial support of this research. They are grateful to N Taibi for the TEM analysis.

Compliance with ethical standards

Conflict of interest The authors declare that they have no conflict of interest.

References

1. Zhang D, Yin Y, Li Y, Cai Y, Liu J (2017) Critical role of natural organic matter in photodegradation of methylmercury in water: molecular weight and interactive effects with other environmental factors. Sci Total Environ 578:535–541
2. Mahmiani Y, Sevim AM, Gül A (2016) Photocatalytic degradation of 4-chlorophenol under visible light by using TiO_2 catalysts impregnated with Co(II) and Zn(II) phthalocyanine derivatives. J Photochem Photobiol A Chem 321:24–32
3. Brahimi R, Bessekhouad Y, Bouguelia A, Trari M (2008) Improvement of eosin visible light degradation using PbS-sensititized TiO_2. J Photochem Photobiol A Chem 194:173–180
4. Bessekhouada Y, Brahimi R, Hamdini F, Trari M (2012) Cu_2S/TiO_2 heterojunction applied to visible light Orange II degradation. J Photochem Photobiol A Chem 248:15–23
5. Tahiri H, Ichou YA, Herrmann JM (1998) Photocatalytic degradation of chlorobenzoic isomers in aqueous suspensions of neat and modified titania. J Photochem Photobiol A Chem 114:219–226
6. Belaissaa Y, Niboua D, Assadi A, Bellal B, Trari M (2016) New hetero-junction *p*-CuO/*n*-ZnO for the removal of amoxicillin by photocatalysis under solar irradiation. J Taiwan Inst Chem Eng 68:254–265
7. Lelarioa F, Brienzaa M, Bufoa SA, Scranob L (2016) Effectiveness of different advanced oxidation processes (AOPs) on the abatement of the model compound mepanipyrim in water. J Photochem Photobiol A Chem 321:187–201
8. Molinari R, Lavorato C, Argurio P (2017) Recent progress of photocatalytic membrane reactors in water treatment and in

synthesis of organic compounds: a review. Catal Today 281:14–164
9. Ali I, Kim SR, Kim SP, Kim JO (2017) Anodization of bismuth doped TiO_2 nanotubes composite for photocatalytic degradation of phenol in visible light. Catal Today 282:31–37
10. Bassaid S, Chaib M, Omeiri S, Bouguelia A, Trar M (2009) Photocatalytic reduction of cadmium over $CuFeO_2$ synthesized by sol-gel. J Photochem Photobiol A Chem 201:62–68
11. Li H, Liu Y, Tang J, Deng Y (2016) Synthesis, characterization and photocatalytic properties of $Mg_{1-x}Zn_xAl_2O_4$ spinel nanoparticles. Solid State Sci 58:14–21
12. Dermèche L, Rabia C, Rekhila G, Trari M (2017) Preparation and characterization of mixed caesium-tin mixed salt of Keggin-type phosphovanadomolybdate. Application to photocatalytic chromate reduction. Sol Energy Mater Sol Cells 168:45–50
13. Bouchaaba H, Bellal B, Maachi R, Trari M, Nasrallaha N, Mellah A (2016) Optimization of physico-chemical parameters for the photo-oxidation of neutral red on the spinel $Co2_SnO_4$. J Taiwan Inst Chem Eng 58:310–317
14. Chen J, Shu J, Anqi Z, Juyuan H, Yan Z, Chen J (2016) Synthesis of carbon quantum dots/TiO_2 nanocomposite for photodegradation of Rhodamine B and cefradine. Diamond Relat Mater 70:137–144
15. Bagtache R, Abdmeziem K, Rekhila G, Trari M (2016) Synthesis and semiconducting properties of Na_2MnPO_4F. Application to degradation of Rhodamine B under UV-light. Mater Sci Semicond Process 51:1–7
16. Fedailaine M, Berkani S, Trari M (2016) Ni^{2+} reduction under solar irradiation over $CuFe_2O_4/TiO_2$ catalysts. J Chem Eng 33:2027–2033
17. Cherifi K, Allalou N, Rekhila G, Trari M, Bessekhouad Y (2015) Nitrate-processing and characterization of a cobalt-doped barium tin oxide perovskite: magnetic, transport and photoelectrochemical properties. Mater Sci Semicond Process 30:571–577
18. Dong H, Li Z, Xu X, Ding Z, Wu L, Wang X, Fu X (2009) Visible light-induced photocatalytic activity of delafossite $AgMO_2$ (M=Al, Ga, In) prepared via a hydrothermal method. Appl Catal B Environ 89:551–556
19. Moualkia H, Rekhila G, Izerrouken M, Mahdjoub A, Trari M (2014) Influence of the film thickness on the photovoltaic properties of chemically deposited CdS thin films: application to the photodegradation of orange II. Mater Sci Semicond Process 21:186–193
20. Rekhila G, Bessekhouad Y, Trari M (2015) Hydrogen evolution under visible light over the solid solution $NiFe_{2-x}Mn_xO_4$ prepared by sol gel. Int J Hydrog Energy 40:12611–12618
21. Benreguia N, Barnabé A, Trari M (2015) Sol-gel synthesis and characterization of the delafossite $CuAlO_2$. J Sol Gel Sci Technol 75:670–679
22. Brahimi R, Bessekhouad Y, Trari M (2012) Physical properties of N_xTiO_2 prepared by sol-gel route. Phys B 407:3897–3904
23. Rekhila G, Bessekhouad Y, Trari M (2016) Synthesis and characterization of the spinel $ZnFe_2O_4$, application to the chromate reduction under visible light. Environ Technol Innova 5:127–135
24. Gómez-Solís C, Peralta-Arriaga SL, Torres-Martínez LM, Juárez-Ramírez I, Díaz-Torres LA (2017) Photocatalytic activity of MAl_2O_4 (M=Mg, Sr and Ba) for hydrogen production. Fuel 188:197–204
25. Gurunathan K, Baeg JO, Lee SM, Subramanian E, Moon SJ, Kong KJ (2008) Visible light active pristine and Fe^{3+} doped $CuGa_2O_4$ spinel photocatalysts for solar hydrogen production Inter. J Hydrog Energy 33:2646–2652
26. Rekhila G, Bessekhouad Y, Trari M (2013) Visible light hydrogen production on the novel ferrite $NiFe_2O_4$. Int J Hydrog Energy 38:6335–6343
27. Pleskov YV (1994) Semiconductor photoelectrochemistry for cleaner environment: utilization of solar energy. Environ Orien Electrochem 59:417–443
28. Amara M, Kerdjoudj H, Bouguelia A, Trari M (2008) A combination between membrane selectivity and photoelectrochemistry to the separation of copper, zinc and nickel in aqueous solutions. J Membr Sci 312:125–131
29. Lahmar H, Rekhila G, Trari M, Bessekhouad Y (2015) $HCrO_4^-$ reduction on the novel heterosystem La_2CuO_4/SnO_2 under solar light. Environ Prog Sustain Energy 34:744–750
30. Belaissaa Y, Niboua D, Assadi AA, Bellal B, Trari M (2016) A new hetero-junction *p*-CuO/*n*-ZnO for the removal of amoxicillin by photocatalysis under solar irradiation. J Taiwan Inst Chem Eng 68:254–265
31. Helaili N, Bessekhouad Y, Bouguelia A, Trari M (2010) *p*-Cu_2O/n-ZnO heterojunction applied to visible light Orange II degradation. Sol Energy 84:1187–1192
32. Arlos MJ, Fraile MMH, Liang R, Bragg LM, Zhou NY, Andrews SA, Servo MR (2016) Photocatalytic decomposition of organic micropollutants using immobilized TiO_2 having different isoelectric points. Water Res 101:351–361
33. Chhor K, Bocquet JF, Colbeau-Justi C (2004) Comparative studies of phenol and salicylic acid photocatalytic degradation: influence of adsorbed oxygen. Mater Chem Phys 86:123–131